A&A 409, 479–484 (2003)
DOI: 10.1051/0004-6361:20031136

Astronomy & Astrophysics

Near-infrared color evolution of LMC clusters⋆

J.-M. Kyeong[1], M.-J. Tseng[2], and Y.-I. Byun[3]

[1] Korea Astronomy Observatory, Taejon, 305-348, Korea
[2] Institute of Astronomy, National Central University, Chung-Li, 32054, Taiwan, ROC
[3] Yonsei University Observatory and Department of Astronomy, Yonsei University, Seoul, 120-749, Korea

Received 5 May 2003 / Accepted 7 July 2003

Abstract. We present here the digital aperture photometry for 28 LMC clusters whose ages are between 5 Myr and 12 Gyr. This photometry is based on our imaging observations in *JHK* and contains integrated magnitudes and colors as a function of aperture radius. In contrast to optical colors, our near-infrared colors do not show any strong dependence on cluster ages.

Key words. galaxies: photometry – galaxies: Magellanic Clouds – galaxies: star clusters – infrared: stars

1. Introduction

Star clusters of the Large Magellanic Cloud (LMC) provide excellent templates for studies of stellar populations in external galaxies. The LMC is close enough that star clusters within the galaxy can be resolved into individual stars by high spatial resolution imaging from both ground and space based telescopes. Their CMDs can be used for detailed age calibration. These star clusters are also populous enough that their integrated colors are less sensitive to stochastic effects when compared to galactic open clusters. Most importantly, unlike globular cluster in our Galaxy, clusters in the LMC are known to cover wide range of ages, making them ideal objects to investigate the integrated spectral behavior of simple stellar population as functions of both age and chemical composition.

Integrated photometry for LMC clusters had been studied since van den Bergh & Hagen (1968), who performed *UBV* photoelectric aperture photometry. In 1980, Searle, Wilkinson and Bagnuolo carried out an extensive program of *uvgr* aperture photometry, which resulted in a classification scheme of age-calibration with the reddening-free parameter $Q(vgr)$ and $Q(ugr)$. This scheme is now called the SWB classification. Their work showed that the integrated colors appear to correlate with cluster ages, and can be used as a primary age indicator. Elson & Fall (1985) translated the SWB classification into the *UBV* two-color diagram and also introduced a reddening independent parameter, *s*, which agrees with the SWB sequence for 90% of clusters. Girardi et al. (1995) revised the relation between the parameter *s* and cluster ages to consider the dispersion of observed colors due to stochastic effects and metallicity variation.

Send offprint requests to: J.-M. Kyeong,
e-mail: jman@kao.re.kr

⋆ Tables 2 and 3 and Fig. 2 are only available in electronic form at http://www.edpsciences.org

Previous effort in near-infrared includes Persson et al. (1983, hereafter Persson83) and Ferraro et al. (1995). Persson83 studied the integrated light of 84 clusters in the Large and Small Magellanic Clouds using a single cell photoelectric aperture photometry. In contrast to the UV and optical clusters colors which vary smoothly with age, their infrared integrated colors display a large scatter among a given SWB classification. They defined a group of IR enhanced clusters that belong to SWB groups IV–VI, i.e., in the intermediate-age with the very red $J-K$ and $H-K$ colors. This color excess is due to the existence of luminous carbon stars on the asymptotic giant branch, which are responsible for as much as half of the bolometric luminosity in the near-infrared.

Ferraro et al. (1995) was the first who used a small, but two-dimensional InSb array for near-infrared observation of LMC clusters. With the classical and overshooting stellar evolution theories, they investigated how red stars dominate the bolometric luminosity of a simple stellar population after its early evolutionary stage. These red stars are considered to be in phase transitions; asymptotic giant branch (AGB) and red giant branch (RGB) branch, in particular. Their overall result is consistent with the earlier work by Persson83. The age dependent variation for $V-K$ (substantially controlled by AGB and RGB stars) shows a large scatter, which makes it almost useless for the purpose of age calibration as well as for the evolutionary study of simple stellar populations.

Using a large format detector which enables more careful background estimates and covers a larger cluster area, we aim to collect a homogeneous data set for LMC clusters in the near-infrared and re-examine the age dependence of integrated infrared color.

This paper is a part of a long term study to understand the broad band color evolution of stellar systems with both simple and more complex stellar populations.

Table 1. Basic properties of LMC clusters in our sample.

NGC	RA(J2000)	Dec	SWB[a]	s^b	log t^c	[Fe/H][d]	$E(B-V)^e$	Dia.[f]	V^g	$B-V^g$	$U-B^g$
1651	04 37 32.1	−70 35 07	V	39	9.30	−0.37	0.11	62V	12.67	0.69	0.30
1711	04 50 37.2	−69 59 03	I	20	7.70	−0.57	0.16	60V	10.11	0.12	−0.37
1783	04 59 10.0	−65 59 14	V	37	9.00	−0.45	0.10	72V	10.93	0.62	0.23
1786	04 59 07.9	−67 44 38	VII	48	10.18	−1.87	0.12	60V	10.88	0.74	0.10
1806	05 02 13.2	−67 59 07	V	40	9.30	−0.23	0.12	88V	11.10	0.73	0.26
1818	05 04 14.8	−66 26 04	I	18	7.40	−0.4~0.0	0.10	72V	9.70	0.18	−0.47
1831	05 06 15.6	−64 55 03	IVA	31	8.50	0.01	0.10	60V	11.18	0.34	0.13
1847	05 07 05.4	−68 58 41	I	21	7.42	−0.37	0.10	72V	11.06	0.20	−0.33
1850	05 08 45.8	−68 45 42	II	21	7.50	−0.12	0.15	50T	9.57	0.15	−0.27
1856	05 09 30.3	−69 08 05	IVA	30	8.12	−0.52	0.24	62V	10.06	0.34	0.07
1866	05 13 39.1	−65 27 56	III	27	8.12	−0.50	0.10	72V	9.73	0.25	−0.04
1868	05 14 35.4	−63 57 16	IVA	33	8.74	−0.50	0.07	62V	11.56	0.45	0.15
1967	05 26 44.3	−69 06 06	I	12	7.00		0.14	50T	10.83	0.05	−0.75
1978	05 28 44.3	−66 14 08	VI	45	9.70	−0.42	0.10	62V	10.70	0.78	0.23
1983	05 27 44.3	−68 59 03	I	13	6.90		0.09	45V	9.94	0.10	−0.76
1987	05 27 18.2	−70 44 05	IVB	35	8.80		0.12	62V	12.08	0.52	0.20
2004	05 30 40.3	−67 17 10	I	15	7.30	−0.56	0.06	72V	9.60	0.17	−0.68
2031	05 33 40.9	−70 59 06	III	27	8.20	−0.52	0.07†	72V	10.83	0.27	-0.05
2074	05 39 01.7	−69 29 51	0	10	6.60		0.07	150T	9.32	-0.16	−0.91
2100	05 42 07.8	−69 12 42	I	17	7.20	−0.32	0.24	60V	9.60	0.16	−0.56
2107	05 43 12.1	−70 38 24	IVA	32	8.60		0.19	60V	11.51	0.38	0.13
2134	05 51 56.7	−71 05 45	III	28	8.00	−1.0	0.10	60V	11.05	0.25	−0.02
2136	05 52 57.7	−69 29 24	III	26	8.00	−0.55	0.10	60V	10.54	0.28	−0.13
2154	05 57 38.3	−67 15 37	V	39	9.20	−0.56	0.10	62V	12.13	0.68	0.30
2155	05 58 34.6	−65 28 36	VI	45	9.51	−0.45	0.10	62V	12.60	0.80	0.23
2157	05 57 34.9	−69 11 45	III	25	7.60	−0.45	0.10	60V	10.16	0.19	−0.16
2164	05 58 56.8	−68 30 56	II	23	7.70	−0.45	0.10	60V	10.34	0.10	−0.24
2214	06 12 58.4	−68 15 33	II	22	7.60	−0.45	0.10	60V	10.93	0.11	−0.27

[a, b] SWB classification and *s* parameter from Bica et al. (1996, hereafter BCDSP96).
[c, d] Logarithmic age and metallicity from Mackey & Gilmore (2003), except for NGC 1651, which is from Sarajedini et al. (2002).
[e] Reddening from Persson83. Except for NGC 1847 from Nelson & Hodge (1983), and NGC 1967, NGC 1983, NGC 2074 from Meurer et al. (1990).
[f] Aperture diameter in arcsec for *BV* photometry. Suffix V and T indicates photometry sources, respectively van den Bergh (1981, hereafter VDB81) and BCDSP96.
[g] Optical photometry data from VDB81 and BCDSP96.
† Adopted mean value across the LMC of $E(B-V) = 0.07$ taken from Burnstein & Heiles (1984).

2. Sample and observation

2.1. Samples

A total of 28 LMC clusters have been selected for our infrared photometry. These clusters were chosen because all of them have been already studied with color–magnitude diagrams (CMD) and cover a wide range of ages from 5 Myr to 12 Gyr as determined by isochrone fitting to the CMDs. Table 1 gives the following basic information for each of our sample clusters.

2.2. Observations

Near-infrared observations were carried out during the nights of Dec. 20–22 in 1996 using the Australian National University 2.3-m telescope and the CASPIR (Cryogenic Array Spectrometer/Imager) instrument at the Siding Spring Observatory. The CASPIR system has InSb 256×256 chip with pixel size of 0.5 arcsec at the Cassegrain focus. We used the double sampling readout mode, whose characteristics can be found in McGregor (1995).

In order to handle possible detector instability and temporal changes of the bright IR background, cluster exposures were taken in a loop sequence. Each loop takes images in the following order ; bias - sky east - cluster - sky west - sky north - cluster - sky south - bias - dark. In most cases, the sky exposures were made in regions about 5 arcmin away from the center of the target cluster in the directions of east, west, north and south. When there was a bright contaminating source in the sky field, we moved the sky into another place nearby. The exposure time was usually 2 s long, except when the cluster has very bright center or stars.

By observing the standard stars in the beginning of the night, at midnight, and again at the end of the night, we attempted to get good sample of calibration data. A set of flatfield frames were obtained using artificial illumination of the inner surface of the dome to correct the pixel-to-pixel sensitivity variations across the array. The domeflat exposures contain a few pairs of lamp-on and lamp-off exposures for each filter, in order to achieve good signal statistics.

Table 2 lists our observation log, including date, cluster name, airmass, exposure time, and comments on the weather condition or centering problem if suspected.

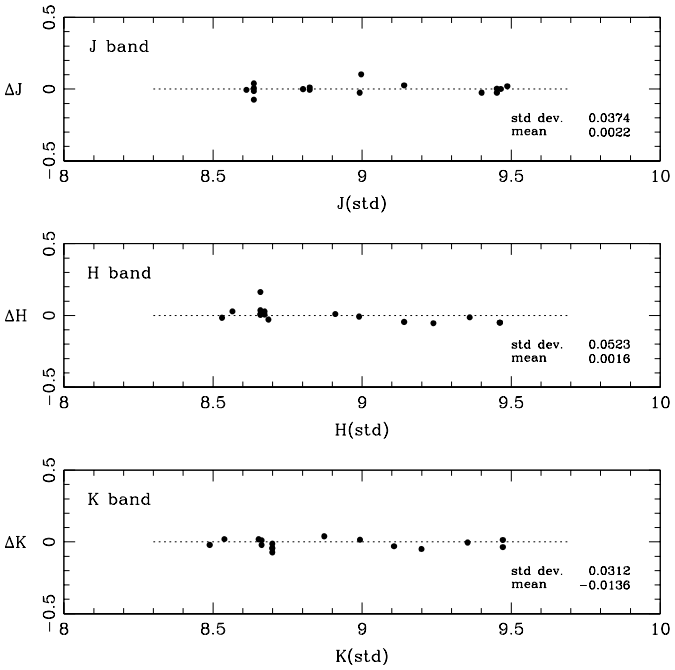

Fig. 1. Residuals between calibrated and standard magnitudes in *J*, *H* and *K*.

3. Data reduction and calibration

We used the IRAF package including MSSSO CASPIR specific routines for basic image processing, and developed a set of software for final digital aperture photometry.

The IR data reduction method is more complex than optical CCD data mainly because of high sky background and its rapid variability. The CASPIR detector array also shows a quadratic non-linearity, which should be linearized to recover the low and high intensity information accurately (McGregor 1995). Each data frame was bias and dark subtracted and, was then median-combined to create a sky frame for that sequence. After subtracting the corresponding sky frames, the data images were subjected to flatfielding.

For each filter, the target clusters are exposed twice. Due to the excellent tracking and pointing capability of the ANU 2.3-m telescope, the two images turned out to be almost exactly aligned without needing an extra step of image relocation. These two images are stacked together by simple averaging. The resulting images are then ready for photometric measurement and analysis.

The instrumental magnitudes of 13 SAAO standard stars (Carter & Meadows 1995) are obtained by digital aperture photometry. The optimal size of aperture was chosen to be 20 pixels in radius after experiments with growth curves. We derived the transformation between our instrument magnitudes and the standard values J, H, K as follows

$$\begin{aligned} j &= J - 19.086(\pm 0.004) + 0.112(\pm 0.004) * X_j \\ &\quad + 0.113(\pm 0.020) * (J - K) \\ h &= H - 18.862(\pm 0.007) + 0.090(\pm 0.014) * X_h \\ k &= K - 18.022(\pm 0.024) + 0.096(\pm 0.019) * X_k \end{aligned}$$

where j, h and k are instrumental magnitudes, X_j, X_h and X_k are airmass. We could not find any significant color term in the H and K bands. Residuals to the standard system are displayed in Fig. 1 and show the accuracy of our calibration.

4. Photometry

4.1. Concentric aperture photometry

Conventional aperture photometry based on photoelectric photometers requires exact centering of the aperture to the cluster center. This can be sometimes a rather difficult task due to contamination of bright stars. It is also difficult to maintain the same position for all the filters if the telescope has to be moved back and forth for sky measurements. The array observations such as ours do not have this problem.

Using fully reduced images, we defined the exact location of our center by examining each image with the following methods. First, we combine all the *JHK* images into one near-IR image and then apply visual inspection. Secondly, we use the BLKAVG task in IRAF to project the two dimensional image into *X*- and *Y*-directions and locate the maximum. Finally, by interactive profile extraction in *X*- and *Y*-direction, using IRAF/imexam, while avoiding bright stars scattered in the cluster field.

The centers determined by the above methods do not differ much. Some exceptions do exist however when there are strong clumps of stars near the general area of cluster center. These clusters are marked as such in Table 2.

After identifying the location of cluster center, we used our privately written program of digital aperture photometry to measure the flux within several apertures of different radii. The results, all converted to standard magnitudes and color are presented in the following section.

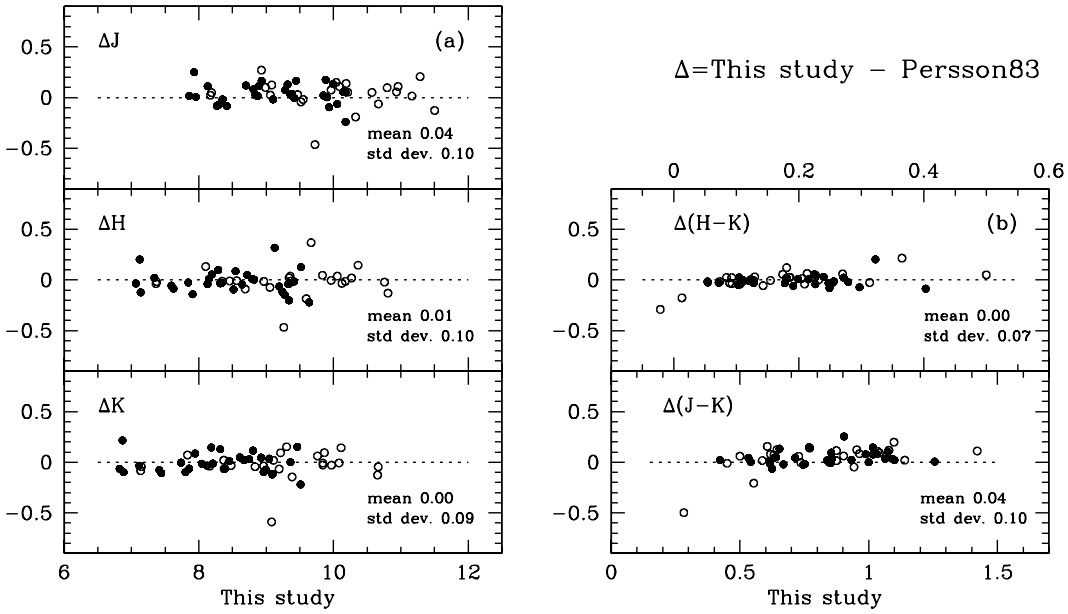

Fig. 3. Comparison with Persson83's photoelectric photometry in J, H, K (**a**), $J-K$, $H-K$ (**b**). Open circles refer to small aperture sizes of 12, 24, 29, 30 and 35 arcsec and filled circles are for bigger apertures of 56, 59, 60, 64, 75 arcsec.

4.2. Results

(a) Magnitude and color profile for each cluster

In order to investigate the radial propagation of integrated magnitudes and colors, we have made multi-aperture concentric photometry with aperture size of 2, 4, 7, 10, 15, 20, 30, 40, 60, 80, 100 arcsec. The J, H and K magnitudes are tabulated in Table 3.

The graphical illustration of magnitude and color are shown in Fig. 2. In the upper panel, the lines with data points are the growth curve of J, H and K, i.e. encircled flux plotted against log R. The error bars are mostly very small and do not show up in the figure except for a few data points. In the lower two panels, the integrated color $J-K$ and $H-K$ are plotted against log R.

As shown in Fig. 2, most clusters show only a small color variation with no big change around diameter 60 arcsec. This tells us that the color with this aperture is representative of each cluster and useful for our purpose.

(b) Comparison with Persson83

In order to see how our data compare with the photometry of Persson83, we performed another set of aperture photometry with apertures of the same size as used by Persson83. The results are illustrated in Fig. 3, which shows the residuals in J, H, K, and also in $J-K$ and $H-K$.

Because Persson83 uses the CIT/CTIO photometric system, we converted their data into our SAAO system using the transformation equations given by Carter (1990).

If there had been serious problem with centering, the discrepancy will be bigger for small apertures. This is because of the strong central concentration of light in clusters and also because the small area coverage will be more subject to an error in using the wrong center. However we do not see any systematically bigger scatter for small aperture measurements. The residuals in H and K bands have mean values close to zero with a scatter less than 0.1 mag, indicating that our photometry is consistent with Persson83.

5. Discussion

With the optical data collected in Table 1 and near-infrared data from Table 3, we present in Fig. 4 the optical and near-IR color variation as a function of cluster age. SWB group boundaries are indicated in the upper part of this diagram. It is apparent that the optical colors $U-B$ and $B-V$ show very strong relation with age. As clusters get older the optical colors get redder almost monotonically. Beyond 1 Gyr, the slope becomes rather flat and even falls off towards the blue. But the latter is probably caused by the oldest cluster NGC 1786 with SWB VII, which has very low metallicity. Compared to the optical colors, the changes in near-IR colors $J-K$ and $H-K$ are not significant nor monotonic.

Persson83 defined the globular clusters with $(J-K)_0 \geq 0.8$, $(H-K)_0 \geq 0.2$ and $(V-K)_0 \geq 2.5$ as "IR enhanced clusters". Within each group of globular and open clusters, there is a tendency that the color becomes bluer as age sequence increases. However, it is not at all the case in our data. Figure 5 shows our data re-plotted for the same colors and for the same scale as in Persson83's Fig. 2. We particularly note the following points;

1. As Persson83 noted, we also find a transition between younger and older clusters. This appears to happen at the age of 100 Myr, which corresponds to the border between SWB II and III. Persson83 on the other hand observed that this happens in SWB IV and V. Our transition is also less abrupt than Persson83's. Among early SWB I and II, the near-infrared colors get somewhat bluer with increasing

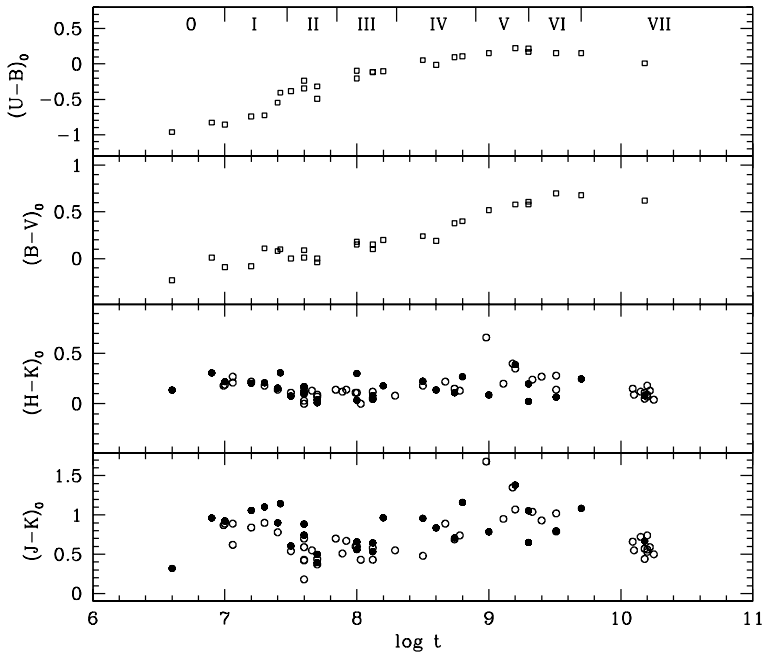

Fig. 4. Optical color evolution (from Searle et al. 1980) and near-infrared color evolution of LMC clusters. Our data (filled circles) are sampled at 60 arcsec diameter and log *t* is from our Table 1. Persson83 data are shown for comparison (open circles). All color are reddening corrected by Bessell & Brett(1988)'s extinction law.

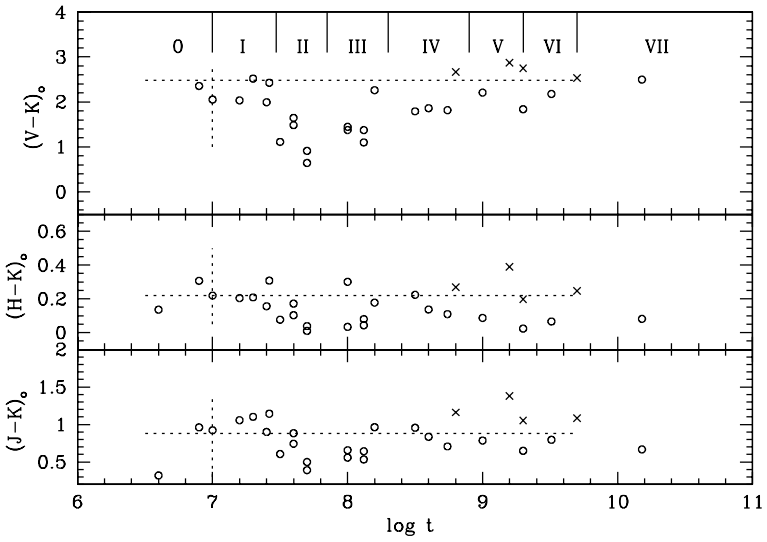

Fig. 5. Our data plotted against log *t* from our Table 1. For near-infrared colors, the data are sampled at 60 arcsec diameter, but for $V-K$ we resampled our near-infrared data to match the *V* aperture given in Table 1. Horizontal dashed line are defined by Persson83 for IR enhanced clusters, shown here after Carter (1990) correction to the SAAO system. Cross symbols indicate 4 clusters classified as IR enhanced by Persson83.

age, while among late SWB types the trend seems to get reversed.

2. Persson83 also noted a substantial population of IR enhanced clusters among old clusters of SWB IV and V. Our data also confirm their existence; our sample includes four of Persson83's IR enhanced clusters and they are all IR bright. However, this IR enhancement does not appear to be limited to a small range of ages. Clusters of comparable IR colors do exist in early SWB types of 0, I and II. These clusters were not included in Persson83's sample.

The near-infrared color vs. age relation has a bigger scatter than in the optical. The origin of scatter in our near-infrared color vs. age relations will be studied in depth after we perform digital stellar photometry on our image data and also after running some color synthesis experiments based on the results of stellar photometry. The most likely cause of the scatter appears to be due to small number statistics for bright and cool giant stars, whose effect is much more pronounced for near-infrared colors.

To sum up, our near-infrared observations suggest that the age dependent variation of infrared color is minor. Also, even if it exists with a small slope, it would be difficult to define the

trend directly from observations for small stellar systems such as LMC clusters. This does not mean that the construction of empirical infrared color evolution is impossible from this data. As suggested above, proper reconstruction of stochastic effects via digital photometry and simulations may prove still useful to define the near-infrared color evolution of stellar systems.

6. Summary

We carried out near-infrared imaging observations for 28 clusters in the LMC. These clusters cover a large span of ages. For each cluster, we performed digital aperture photometry with several different circular apertures and presented here the magnitudes and colors as a function of aperture size. The precision of our data has been checked internally with standard star observations and externally with previous photoelectric observations of Persson83 after proper filter correction.

The age dependence of near-infrared integrated color appears to be much smaller compared to that of optical colors. We also find the presence of a slope transient near 100 Myrs. Our color–age relationship shows a scatter much bigger than those of optical correlations. Presently we interpret this as a result of statistical effects involved with small numbers of bright and cool giant stars in the small stellar systems such as LMC clusters.

Population synthesis and Monte Carlo modelling of stochastic effects (e.g. Santos & Frogel 1997) can be a useful approach to the problem. In our subsequent work, however, we will estimate the stochastic effect in a more direct way by detailed study of digital stellar photometry using the present array data.

Acknowledgements. We gratefully acknowledge the careful reading and suggestions made by our referee R. A. Johnson. We also would like to thank the staff of the Australian National University for their help during our observing run at the Siding Spring Observatory. This research was supported by Korean Research Foundation Grant (KRF-2000-015-DP0445).

References

Bessell, M. S., & Brett, J. M. 1988, PASP, 100, 1134
Bica, E., Claria, J. J., Doyyori, H., Santos, J. F. C., Jr., & Piatti, A. E. 1996, ApJS, 102, 57 (BCDSP96)
Burnstein, D., & Heiles, C. 1984, ApJS, 54, 33
Carter, B. S. 1990, MNRAS, 242, 1
Carter, B. S., & Meadows, V. S. 1995, MNRAS, 276, 734
Elson, R. A. W., & Fall, S. M. 1985, ApJ, 299, 211
Ferraro, F. R., Fusi Pecci, F., Testa, V., et al. 1995, MNRAS, 272, 391
Girardi, L., Chiosi, C., Bertelli, G., & Bressan, A. 1995, A&A, 298, 87
Mackey, A. D., & Gilmore, G. F., 2003, MNRAS, 338, 85
McGregor, P. J. 1995, Users Manual for the Cryogenic Array Spectrometer/Imager (CASPIR) on the MSSSO 2.3 m Telescope
Meurer, G. R., Cacciari, C., & Freeman, F. C. 1990, AJ, 99, 1124
Nelson, M., & Hodge, P. 1983, PASP, 95, 5
Persson, S. E., Aaronson, M., Cohen, J. G., Frogel, J. A., & Matthews, K. 1983, ApJ, 266, 105 (Persson83)
Santos, J. F., & Frogel, J. A. 1997, ApJ, 479, 764
Sarajedini, A., Grocholski, A. J., Levine, J., & Lada, E. 2002, AJ, 124, 2625
Searle, L., Wilkinson, A., & Bagnuolo, W. G. 1980, ApJ, 239, 803
van den Bergh, S. 1981, A&AS, 46, 79 (VDB81)
van den Bergh, S., & Hagen, G. L. 1968, AJ, 73, 569

Online Material

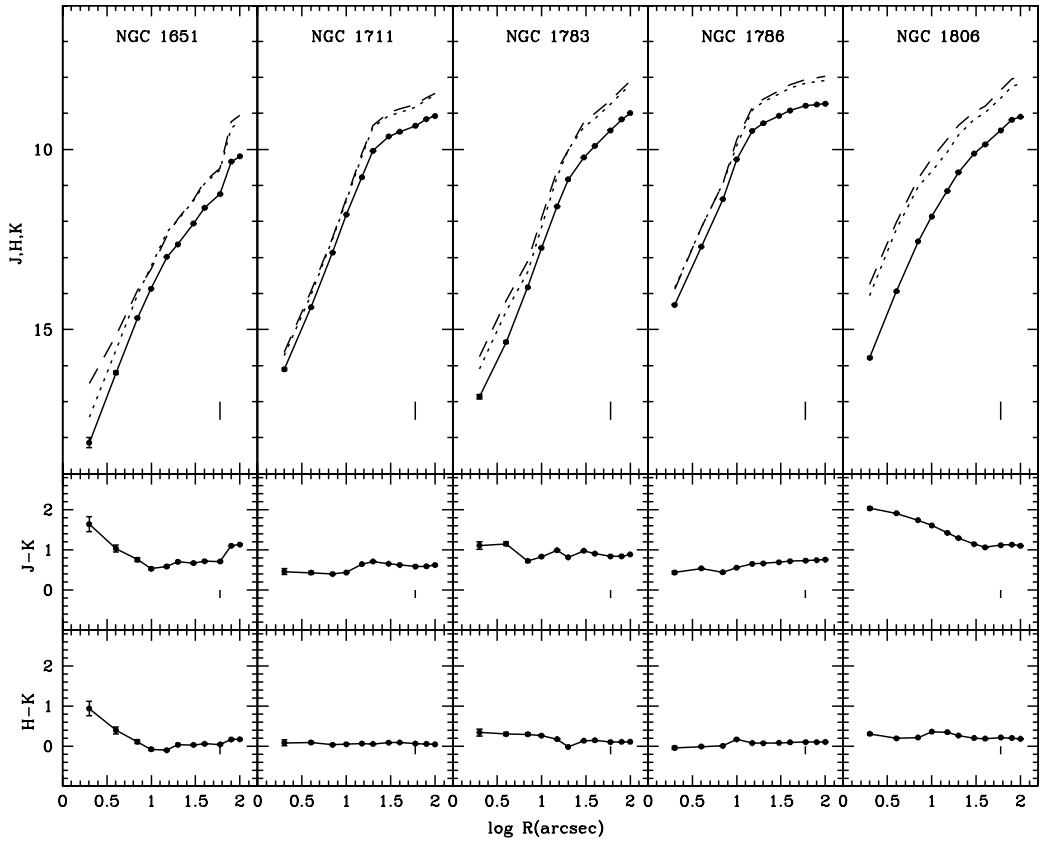

Fig. 2. Magnitude and color profiles of LMC clusters. In upper panel solid line represents *J*, dotted line for *H*, dashed line for *K*. Straight vertical line indicates the location of $R = 60$ arcsec.

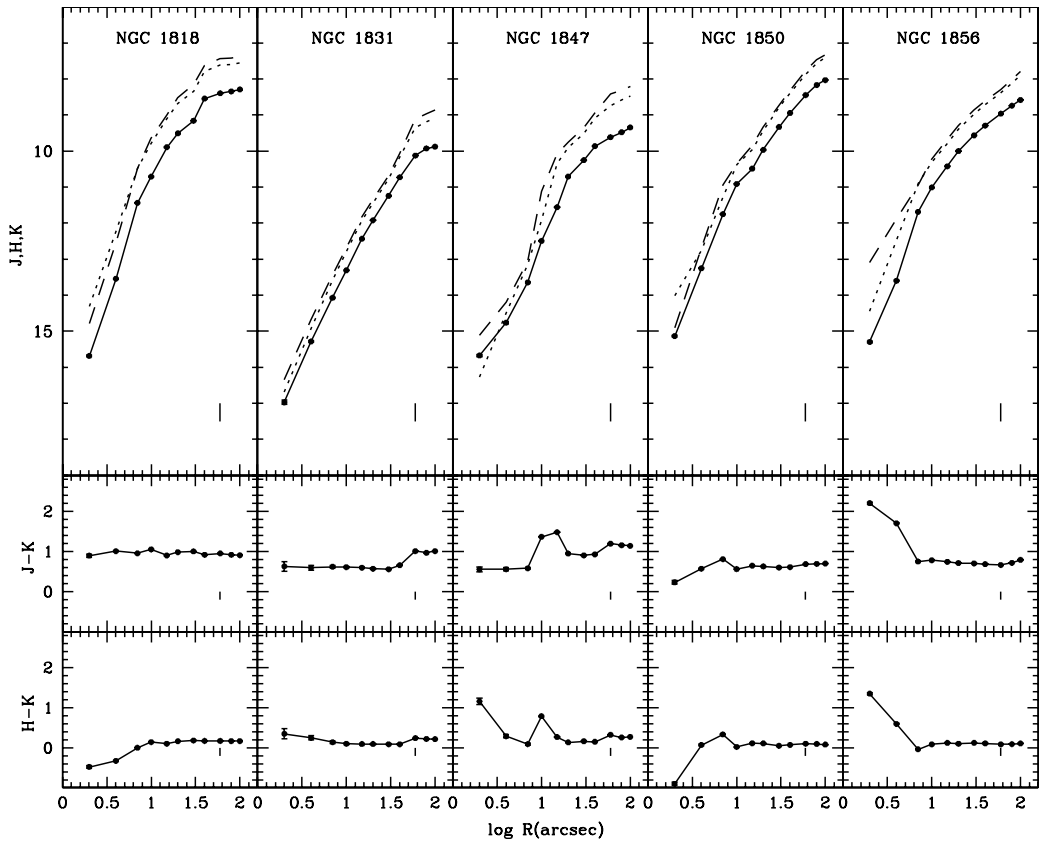

Fig. 2. continued.

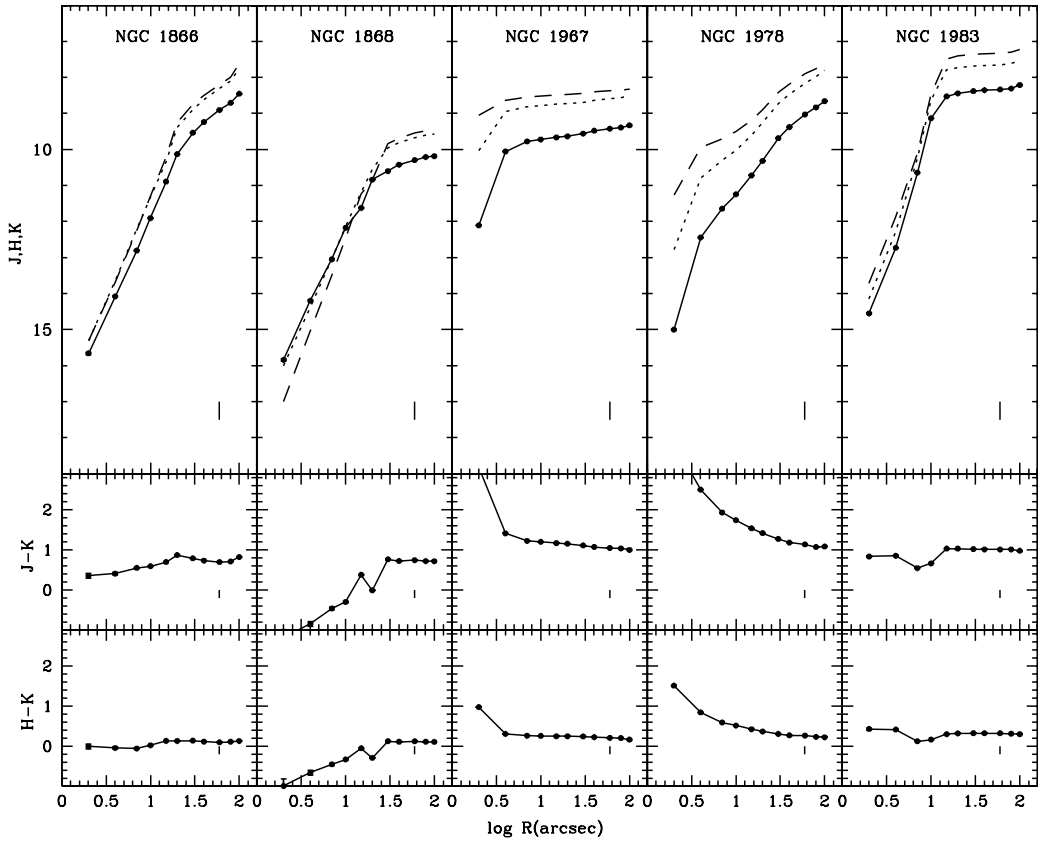

Fig. 2. continued.

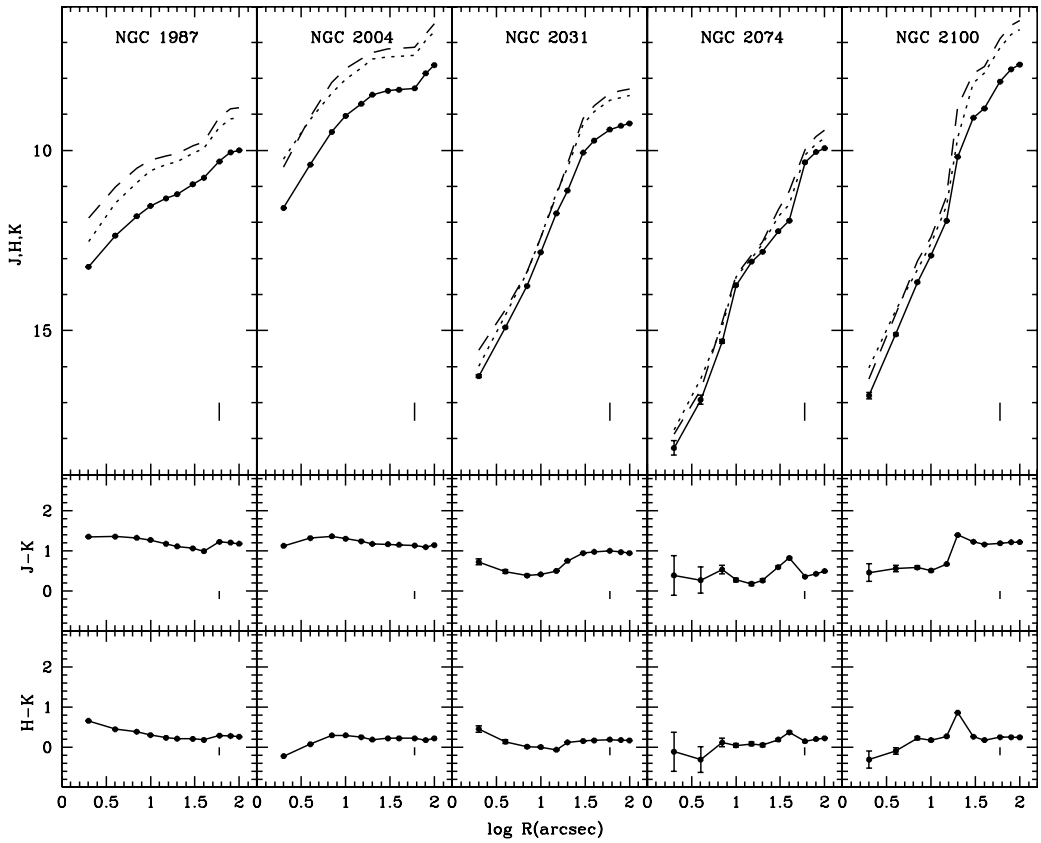

Fig. 2. continued.

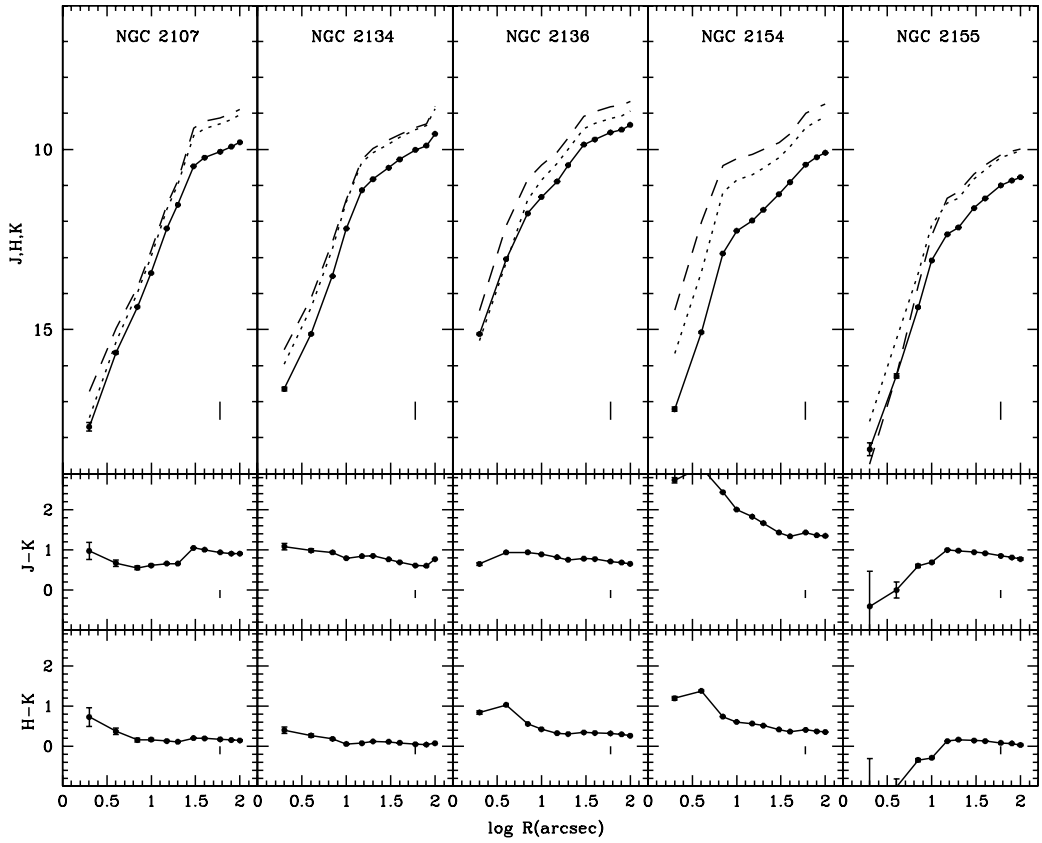

Fig. 2. continued.

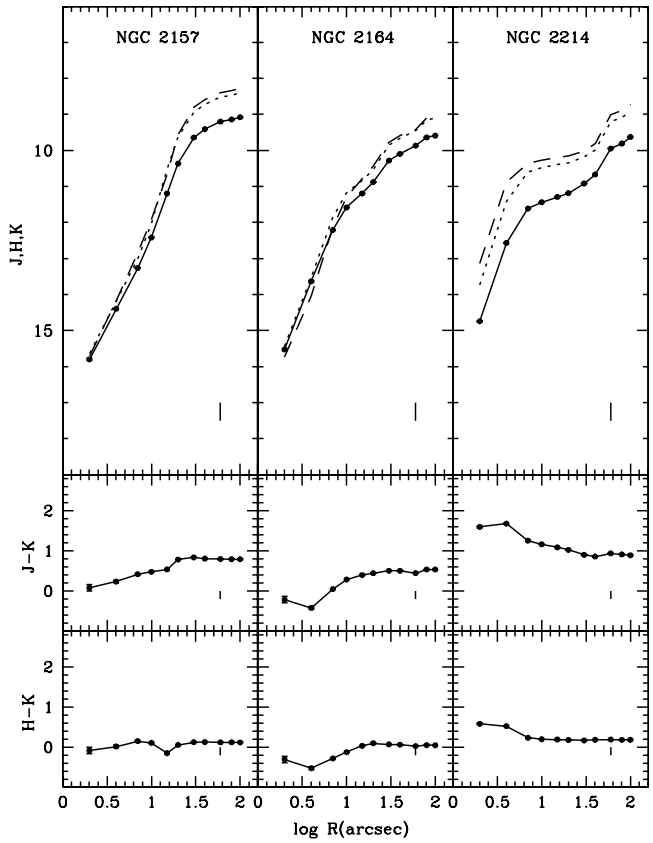

Fig. 2. continued.

Table 2. Observing log.

NGC	Date	Airmass	Exp. (s)	Comments
1651	96 Dec 20	1.295	2	
1711	20	1.410	2	
1783	20	1.246	2	
1786	21	1.327	0.5	
1806	20	1.544	2	
1818	20	1.225	2	
1831	20	1.210	2	b, d
1847	21	1.308	2	
1850	20	1.324	2	
1856	21	1.410	2	
1866	20	1.231	2	
1868	21	1.188	2	
1967	21	1.369	2,0.5,0.3	
1978	21	1.235	2	
1983	20	1.311	2	
1987	22	1.341	2	b
2004	21	1.378	1	b
2031	20	1.449	2	c
2074	21	1.335	2	a
2100	21	1.434	1	c
2107	21	1.294	2	eN
2134	20	1.379	2	b
2136	22	1.291	2	d
2154	22	1.364	2	
2155	22	1.260	2	
2157	21	1.445	2	
2164	22	1.512	2	
2214	22	1.475	2	

a Centering difficult due to sparse field.
b Centering might be influenced by a bright star.
c Centering might be influenced by numerous bright stars.
d Cloudy and/or bad seeing.
eN Changing sky location toward North.

Table 3. Concentric aperture photometry for each cluster.

Dia.(″)	*J*	*H*	*K*	*J*	*H*	*K*	*J*	*H*	*K*
NGC		1651			1711			1783	
2	18.138	17.433	16.494	16.100	15.724	15.637	16.861	16.093	15.747
4	16.197	15.557	15.160	14.379	14.040	13.945	15.344	14.495	14.190
7	14.676	14.025	13.914	12.865	12.500	12.463	13.827	13.400	13.100
10	13.867	13.259	13.334	11.807	11.422	11.369	12.732	12.163	11.897
15	12.980	12.292	12.391	10.772	10.193	10.124	11.582	10.764	10.588
20	12.634	11.964	11.927	10.039	9.384	9.326	10.829	9.996	10.012
30	12.053	11.412	11.379	9.638	9.071	8.981	10.221	9.378	9.240
40	11.621	10.960	10.900	9.509	8.974	8.879	9.899	9.135	8.987
60	11.237	10.570	10.525	9.341	8.821	8.752	9.473	8.737	8.631
80	10.338	9.402	9.233	9.156	8.623	8.562	9.164	8.430	8.321
100	10.189	9.228	9.055	9.071	8.493	8.444	8.990	8.211	8.100
NGC		1786			1806			1818	
2	14.313	13.835	13.874	15.783	14.056	13.745	15.686	14.314	14.787
4	12.698	12.151	12.157	13.936	12.218	12.019	13.542	12.209	12.531
7	11.378	10.945	10.934	12.551	11.026	10.809	11.436	10.483	10.479
10	10.274	9.887	9.715	11.862	10.614	10.252	10.709	9.797	9.652
15	9.485	8.910	8.830	11.151	10.076	9.724	9.891	9.092	8.987
20	9.272	8.684	8.607	10.635	9.605	9.337	9.506	8.686	8.519
30	9.066	8.457	8.370	10.114	9.173	8.967	9.156	8.334	8.149
40	8.919	8.295	8.197	9.859	8.984	8.792	8.542	7.795	7.620
60	8.785	8.154	8.050	9.469	8.570	8.349	8.395	7.614	7.439
80	8.753	8.110	8.007	9.176	8.251	8.043	8.344	7.593	7.422
100	8.732	8.079	7.972	9.093	8.175	7.989	8.289	7.549	7.379
NGC		1831			1847			1850	
2	16.972	16.690	16.338	15.674	16.274	15.114	15.134	14.005	14.899
4	15.284	14.936	14.686	14.760	14.488	14.196	13.253	12.752	12.679
7	14.071	13.590	13.449	13.643	13.154	13.059	11.751	11.273	10.938
10	13.310	12.802	12.697	12.493	11.913	11.123	10.912	10.372	10.347
15	12.435	11.931	11.835	11.558	10.344	10.074	10.485	9.950	9.835
20	11.919	11.439	11.344	10.708	9.894	9.755	9.964	9.444	9.332
30	11.241	10.769	10.679	10.253	9.515	9.347	9.331	8.780	8.727
40	10.728	10.160	10.068	9.861	9.083	8.929	8.943	8.402	8.328
60	10.123	9.354	9.111	9.615	8.742	8.415	8.444	7.859	7.754
80	9.927	9.181	8.956	9.476	8.577	8.316	8.166	7.569	7.470
100	9.877	9.082	8.864	9.344	8.477	8.200	8.028	7.408	7.324

Table 3. continued.

Dia.(″)	*J*	*H*	*K*	*J*	*H*	*K*	*J*	*H*	*K*
NGC		1856			1866			1868	
2	15.297	14.440	13.089	15.660	15.299	15.302	15.839	16.009	16.999
4	13.598	12.488	11.891	14.078	13.625	13.666	14.198	14.380	15.039
7	11.687	10.899	10.934	12.807	12.196	12.251	13.048	13.054	13.505
10	11.009	10.311	10.223	11.905	11.333	11.308	12.172	12.138	12.467
15	10.421	9.799	9.675	10.892	10.326	10.192	11.622	11.189	11.240
20	10.000	9.390	9.284	10.129	9.388	9.255	10.836	10.552	10.843
30	9.563	8.981	8.855	9.536	8.883	8.743	10.601	9.962	9.835
40	9.291	8.714	8.602	9.239	8.618	8.503	10.421	9.809	9.696
60	8.961	8.382	8.293	8.905	8.304	8.205	10.295	9.671	9.548
80	8.739	8.112	8.018	8.708	8.107	7.994	10.210	9.601	9.488
100	8.581	7.895	7.785	8.455	7.762	7.631	10.187	9.574	9.466
NGC		1967			1978			1983	
2	12.107	10.033	9.058	15.000	12.773	11.264	14.550	14.143	13.713
4	10.055	8.948	8.640	12.442	10.782	9.939	12.731	12.292	11.875
7	9.778	8.812	8.549	11.643	10.301	9.708	10.643	10.218	10.094
10	9.722	8.777	8.519	11.245	10.019	9.503	9.134	8.634	8.468
15	9.665	8.743	8.494	10.719	9.604	9.179	8.527	7.795	7.493
20	9.635	8.727	8.478	10.317	9.265	8.897	8.443	7.728	7.408
30	9.558	8.690	8.445	9.688	8.718	8.411	8.381	7.685	7.359
40	9.480	8.631	8.404	9.378	8.467	8.194	8.354	7.663	7.339
60	9.424	8.584	8.374	9.027	8.154	7.888	8.336	7.648	7.324
80	9.392	8.556	8.352	8.831	7.990	7.756	8.309	7.607	7.294
100	9.332	8.496	8.330	8.659	7.797	7.572	8.211	7.532	7.230
NGC		1987			2004			2031	
2	13.228	12.530	11.873	11.596	10.247	10.467	16.263	15.993	15.537
4	12.364	11.456	11.007	10.396	9.147	9.073	14.909	14.558	14.420
7	11.827	10.887	10.500	9.485	8.414	8.118	13.763	13.389	13.376
10	11.540	10.569	10.266	9.040	8.030	7.734	12.825	12.411	12.407
15	11.331	10.390	10.153	8.708	7.717	7.466	11.747	11.181	11.245
20	11.214	10.311	10.097	8.454	7.469	7.279	11.115	10.483	10.362
30	10.938	10.082	9.873	8.345	7.398	7.177	10.061	9.268	9.114
40	10.760	9.947	9.766	8.316	7.382	7.161	9.726	8.917	8.748
60	10.306	9.369	9.078	8.277	7.361	7.141	9.421	8.608	8.417
80	10.053	9.125	8.844	7.861	6.941	6.765	9.316	8.525	8.345
100	9.995	9.076	8.814	7.631	6.705	6.484	9.249	8.471	8.300

Table 3. continued.

Dia.(″)	*J*	*H*	*K*	*J*	*H*	*K*	*J*	*H*	*K*
NGC		2074			2100			2107	
2	18.258	17.756	17.867	16.804	16.036	16.343	17.697	17.450	16.721
4	16.917	16.336	16.643	15.104	14.443	14.540	15.638	15.334	14.964
7	15.298	14.879	14.762	13.656	13.296	13.067	14.369	13.968	13.813
10	13.741	13.508	13.462	12.916	12.582	12.404	13.430	12.984	12.817
15	13.084	12.991	12.904	11.952	11.550	11.279	12.191	11.657	11.527
20	12.812	12.603	12.548	10.178	9.643	8.780	11.535	10.984	10.873
30	12.242	11.833	11.642	9.095	8.129	7.865	10.466	9.618	9.414
40	11.949	11.497	11.125	8.836	7.852	7.673	10.227	9.417	9.221
60	10.328	10.118	9.969	8.090	7.148	6.898	10.063	9.294	9.121
80	10.043	9.817	9.613	7.746	6.777	6.528	9.921	9.165	9.011
100	9.937	9.663	9.439	7.617	6.643	6.396	9.801	9.035	8.891
NGC		2134			2136			2154	
2	16.645	15.957	15.555	15.123	15.311	14.469	17.206	15.660	14.465
4	15.123	14.405	14.136	13.046	13.140	12.107	15.073	13.387	12.007
7	13.514	12.759	12.574	11.777	11.393	10.834	12.885	11.184	10.445
10	12.196	11.457	11.400	11.318	10.851	10.426	12.257	10.854	10.250
15	11.131	10.362	10.285	10.888	10.395	10.069	11.972	10.707	10.141
20	10.826	10.093	9.972	10.433	9.982	9.676	11.678	10.521	10.008
30	10.508	9.852	9.739	9.864	9.426	9.080	11.241	10.224	9.806
40	10.276	9.668	9.581	9.723	9.280	8.948	10.908	9.932	9.568
60	10.011	9.450	9.397	9.528	9.135	8.815	10.421	9.394	8.985
80	9.891	9.327	9.285	9.451	9.061	8.763	10.217	9.222	8.851
100	9.568	8.870	8.794	9.318	8.926	8.663	10.091	9.094	8.740
NGC		2155			2157			2164	
2	18.324	17.548	18.729	15.797	15.631	15.712	15.523	15.435	15.737
4	16.291	15.278	16.292	14.396	14.176	14.157	13.630	13.527	14.048
7	14.379	13.434	13.775	13.263	12.996	12.843	12.208	11.880	12.160
10	13.080	12.100	12.388	12.417	12.044	11.936	11.582	11.171	11.292
15	12.353	11.482	11.354	11.194	10.508	10.654	11.192	10.827	10.792
20	12.165	11.347	11.182	10.365	9.633	9.577	10.878	10.533	10.434
30	11.628	10.825	10.683	9.643	8.928	8.802	10.283	9.847	9.776
40	11.358	10.569	10.440	9.408	8.727	8.598	10.095	9.656	9.590
60	10.997	10.230	10.145	9.198	8.520	8.398	9.867	9.448	9.419
80	10.863	10.119	10.049	9.140	8.467	8.344	9.637	9.152	9.099
100	10.769	10.025	9.993	9.078	8.402	8.283	9.587	9.099	9.049

Table 3. continued.

Dia.(″)	*J*	*H*	*K*
NGC		2214	
2	14.740	13.724	13.140
4	12.566	11.407	10.883
7	11.611	10.589	10.354
10	11.437	10.473	10.272
15	11.290	10.391	10.199
20	11.183	10.337	10.155
30	10.917	10.184	10.012
40	10.668	9.993	9.807
60	9.946	9.197	9.006
80	9.808	9.078	8.893
100	9.626	8.917	8.731